Cooperative Binding of Midazolam with Testosterone and α-Naphthoflavone within the CYP3A4 Active Site: A NMR T_1 Paramagnetic Relaxation Study†

Michael D. Cameron, Bo Wen, Kyle E. Allen, Arthur G. Roberts, Jason T. Schuman, A. Patricia Campbell, Kent L. Kunze, and Sidney D. Nelson*

Department of Medicinal Chemistry, University of Washington, Box 357610, Seattle, Washington 98195

Received August 24, 2005; Revised Manuscript Received September 9, 2005

ABSTRACT: Recent studies have indicated that CYP3A4 exhibits non-Michaelis−Menten kinetics for numerous substrates. Both homo- and heterotropic activation have been reported, and kinetic models have suggested multiple substrates within the active site. We provide some of the first physicochemical data supporting the hypothesis of allosteric substrate binding within the CYP3A4 active site. Midazolam (MDZ) is metabolized by CYP3A4 to two hydroxylated metabolites, 1′- and 4-hydroxymidazolam. Incubations using purified CYP3A4 and MDZ showed that both α-naphthoflavone (α-NF) and testosterone affect the ratio of formation rates of 1′- and 4-hydroxymidazolam. Similar to previous reports, α-NF was found to promote formation of 1′-hydroxymidazolam, while testosterone stimulated formation of 4-hydroxymidazolam. NMR was used to measure the closest approach of individual MDZ protons to the paramagnetic heme iron of CYP3A4 using paramagnetic T_1 relaxation measurements. Solutions of 0.2 μM CYP3A4 with 500 μM MDZ resulted in calculated distances between 7.4 and 8.3 Å for all monitored MDZ protons. The distances were statistically equivalent for all protons except C3−H and were consistent with the rotation within the active site or sliding parallel to the heme plane. When 50 μM α-NF was added, proton−heme iron distances ranged from 7.3 to 10.0 Å. Consistent with kinetics of activation, the 1′ position was situated closest to the heme, while the fluorophenyl 5-H proton was the furthest. Proton−heme iron distances for MDZ with CYP3A4 and 50 μM testosterone ranged from 7.7 to 9.0 Å, with the flourophenyl 5-H proton furthest from the heme iron and the C4-H closest to the heme, also consistent with kinetic observations. When titrated with CYP3A4 in the presence of MDZ, testosterone and α-NF resonances themselves exhibited significant broadening and enhanced relaxation rates, indicating that these effector molecules were also bound within the CYP3A4 active site near the paramagnetic heme iron. These results suggest that the effector exerts its cooperative effects on MDZ metabolism through simultaneous binding of MDZ and effector near the CYP3A4 heme.

Allosterism with cytochromes P450 was first proposed to explain the observed kinetics of steroid metabolism in the presence of α-naphthoflavone (α-NF)[1] (*1*, *2*). Subsequently, several studies have shown both homo- and heterotropic effects on cytochrome P450 3A4 (CYP3A4) (*3*−*13*). CYP3A4 is the major human hepatic P450 and has a large and diverse array of substrates that it oxidizes (*14*). Understanding the nature of allosteric interactions with CYP3A4 may improve the ability to predict what types of compounds are likely to contribute to drug−drug interactions.

A major step toward this goal has recently been achieved with the determination of high-resolution structures by X-ray crystallography of modified soluble forms of human CYP3A4 (*15*, *16*). However, to date, only fluorescence emission spectroscopy of pyrene complexes has provided physicochemical evidence for allosteric interactions of CYP3A4 substrates within the active site (*17*). Kinetic models have been proposed to explain the observed allosterism (*3*, *5*, *9*−*11*, *18*), as well as theoretical molecular models (*13*). These reports have proposed an allosteric interaction within the CYP3A4 active site. The models have tried to differentiate between two substrates simultaneously bound to the active site, substrates competing for the active site, and changes induced by binding of an effector at a site other than the active site. However, limited data is available on physical changes at the active site upon the addition of the allosteric partner.

Midazolam (MDZ, see Figure 1) metabolism by CYP3A4 yields two products, 1′- and 4-hydroxymidazolam. At MDZ concentrations below 25 μM, the predominant product is the 1′-hydroxy metabolite. At higher concentrations, the rate of 4-hydroxylation increases and the rate of 1′-hydroxylation decreases from what is seen at 25 μM. The observed decrease in 1′-hydroxymidazolam formation at higher MDZ concentrations is consistent with a negative homotropic allosteric interaction.

Site-directed mutagenesis has been used to modify the proposed MDZ substrate-binding regions (*12*). The catalytic

† This work was supported by NIH Grant GM32165 (to S.D.N.) and the University of Washington NIEHS sponsored Center for Ecogenetics and Environmental Health: NIEHS P30ES07033.

* To whom correspondence should be addressed: Department of Medicinal Chemistry, University of Washington, Box 357610, Seattle, WA 98195. Telephone: (206) 543-1419. Fax: (206) 685-3252. E-mail: sidnels@u.washington.edu.

[1] Abbreviations: CYP3A4, cytochrome P450 3A4; α-NF, α-naphthoflavone; MDZ, midazolam.

10.1021/bi051689t CCC: $30.25
Published on Web 10/07/2005

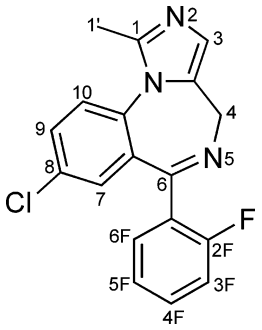

FIGURE 1: Structure of MDZ, 8-chloro-6-(2-fluorophenyl)-1-methyl-4H-imidazo[1,5-a][1,4]benzodiazepine.

efficiency of MDZ oxidation by CYP3A4 could be altered in favor of either the 1′-hydroxy or the 4-hydroxy metabolite. This study and others provide support for two or more possible MDZ-binding sites, with at least one that favored the 1′-hydroxy metabolite and one that favored the formation of the 4-hydroxy metabolite. It is possible that effectors such as testosterone and α-NF bind in sites that effectively block access to at least one but not all of the possible MDZ-binding sites, an effect that would be consistent with the mutation study of Khan et al. (*12*). However, point mutations can lead to structural changes beyond their immediate locale; thus, other kinds of studies are needed to identify positions of effector binding.

NMR T_1 paramagnetic relaxation studies rely on the principle of enhanced relaxation rates of nuclei via the interaction with unpaired electrons, in this case, the protons of MDZ with the unpaired electrons of the high-spin paramagnetic ferric heme iron. The gyromagnetic moment of the electrons of high-spin ferric iron is roughly 10^3 times larger than the gyromagnetic moment of the protons. Thus, because paramagnetic relaxation rates are a function of the squares of the proton and electron magnetic moments (*19*), the paramagnetic contribution to nuclear relaxation can be significant, even for exchanging systems where a low concentration of paramagnetic agent is present (a low concentration of CYP3A4 in the current study). The paramagnetic contribution can be correlated to distances between the proton and the paramagnetic center using the Solomon−Bloembergen equation (*20*−*22*). Because the relationship between the distance and enhanced relaxation rate is sixth order, while time and enhanced relaxation is first order, calculated distances more accurately reflect the closest approach of any given proton to the paramagnetic center than the average position of the proton relative to the heme.

T_1 paramagnetic relaxation experiments have recently been used to demonstrate that dapsone, as an effector, alters the orientation of flurbiprofen within the active site of CYP2C9, thereby increasing the rate of 4′-hydroxylation of flurbiprofen (*23*). The use of T_1 paramagnetic relaxation experiments are well-suited to probe CYP3A4−MDZ allosterism. First, MDZ solubility in water allows for the use of sufficient substrate concentrations for NMR relaxation measurements. Many CYP3A4 substrates are sparingly soluble in aqueous solutions. Second, MDZ has numerous nonexchangeable protons with nonoverlapping NMR signals that allows the molecule to be positioned with respect to the heme iron. Finally, MDZ oxidation has been studied previously *in vitro* using both human microsomes and recombinant holoenzymes. Thus, physiochemical results of this study can be extrapolated to the results of kinetic studies in more physiological systems.

MATERIALS AND METHODS

Chemicals Used. Deuterated solvents were purchased from Cambridge Isotope Laboratories (Andover, MA). Chelex 100 resin was purchased from Bio-Rad (Hercules, CA). Lipids were purchased from Avanti Polar Lipids, Inc. (Alabaster, AL). MDZ was provided as a gift from Roche Pharmaceuticals (Nutley, NJ). Other chemicals were purchased from Sigma Chemical Co. (St. Louis, MO) in the highest purity available. All solutions were prepared from Mili-Q-treated water with a specific resistance ≤17.8 MΩ or 99.9% D_2O as purchased.

Production of Purified CYP3A4. Recombinant CYP3A4 was produced in *Escherichia coli* DH5α using the expression vector pCW 3A4-His6 kindly provided by Dr. Ron Estabrook. In a 2.8 L Fernbach flask, cells were shaken at 150 rpm and 27 °C for 48 h. Media and remaining expression conditions are as described by Gillam et al. (*24*). Pelleted cells were resuspended in resuspension buffer: 100 mM Tris-HCl at pH 7.4, 50 μM testosterone, 20% glycerol, and protease inhibitor cocktail from Sigma Chemical Co. (1 mL/L of initial culture volume). Lysozyme (5 mg/L of culture) was added and allowed to stir at 4 °C for 1 h. Cells were homogenized and spun at 150000*g*, and the yellowish supernatant was discarded. The pellet was resuspended in resuspension buffer by homogenization and allowed to stir at 4 °C for 1 h after the addition of 1% Emulgen 911. The solution was centrifuged at 150000*g*. The red/orange supernatant had imidazole added to a final concentration of 25 mM and was directly loaded onto ProBond nickel resin from Invitrogen. The column was washed with 20 column volumes of wash buffer: 100 mM Tris-HCl at pH 7.4, 20% glycerol, 40 mM imidazole, 0.05% cholate, and 50 μM testosterone. The column was then eluted with a minimal volume of elution buffer: 100 mM Tris-HCl at pH 7.4, 20% glycerol, 500 mM imidazole, and 0.02% cholate. The eluted protein was dialyzed against 100 mM potassium phosphate at pH 7.4 in 20% glycerol and stored at −80 °C. Final yields after purification were typically 200 nmol/L of culture.

Expression and Purification of Cytochrome b5 and NADPH−Cytochrome P450 Oxidoreductase. Both cytochrome *b*5 and NADPH−cytochrome P450 oxidoreductase were expressed in *E. coli*. Human cytochrome *b*5 expression plasmid was provided by Dr. Ron Estabrook and expressed in BL21-DE3 cells using previously described conditions (*25*). Purification of cytochrome *b*5 was similar to the purification of CYP3A4. Expression and purification of NADPH−cytochrome P450 oxidoreductase was as described by Chen et al. (*26*).

Incubations. Premixes for CYP3A4 were prepared using a protocol described elsewhere (*27*). Briefly, two stock solutions, a 5× protein premix and a 5× buffer premix, were prepared into 500 μL fractions and frozen at −80 °C. Final concentrations for the 5× protein premix were 0.5 μM CYP3A4, 1.0 μM NADPH−cytochrome P450 reductase, 0.5 μM cytochrome *b*5, 0.5 mg/mL CHAPS, 0.033 mg/mL of L-α-dilauroyl-*sn*-glycero-3-phosphocholine (DLPC), 0.033 mg/mL of L-α-dioleoyl-*sn*-glycero-3-phosphocholine (DOPC), 0.033 mg/mL of L-α-dilauroyl-*sn*-glycero-3-phosphoserine

(DLPS), and 3 mM GSH in 50 mM potassium HEPES buffer at pH 7.4. All three enzymes were dialyzed to remove glycerol from the enzyme storage buffers before preparation of the premix. The final concentration of the 5× buffer premix was 12 mM GSH and 150 mM $MgCl_2$ in 200 mM potassium HEPES buffer at pH 7.4.

Incubations contained 20 μL of both premixes and 60 μL of water containing the substrate. The reactions were initiated by the addition of NADPH (1 mM final concentration). After 3 min at 37 °C, the reactions were stopped by adding 50 μL of acetonitrile containing internal standards (120 ng/mL $^{15}N_3$-$^2H_7$-MDZ and $^2H_2$-1′-hydroxymidazolam) and centrifuged at 16000*g* for 5 min to precipitate the protein. The MDZ metabolites were assayed by LC−MS/MS using a Zorbax SB-C8 (2.1 × 50 mm, 5 μm particle size) column and an initial mobile phase of 55% water and 0.2% acetic acid and 45% methanol and 0.2% acetic acid. A gradient was run over 2 min to 80% methanol. A Micromass Quattro II/MassLynx NT DS in MRM mode was used for detection of the metabolites by monitoring the following mass transitions: primary, *m*/*z* 326; secondary, *m*/*z* 291 (MDZ); primary, *m*/*z* 336; secondary, *m*/*z* 301 for the MDZ internal standard ($^{15}N_3$-$^2H_7$-MDZ); primary, *m*/*z* 342; secondary, *m*/*z* 203 (1′-hydroxymidazolam); primary, *m*/*z* 346; secondary, *m*/*z* 207 for the ^{37}Cl isotope of $^2H_2$-1′-hydroxymidazolam; and primary, *m*/*z* 342; secondary, *m*/*z* 325 (4-hydroxymidazolam). Ratios of the metabolite to the internal standard were used for quantitation.

NMR Characterization of MDZ. NMR resonance signals for MDZ were assigned at 750 MHz, using a Bruker Advance DMX750 spectrometer. MDZ (10 mg) was dissolved in 0.5 mL of methanol-d_4 and transferred to a standard 5 mm NMR tube. The ^{1}H NMR, ROESY, HSQC, and HMBC spectra were acquired at room temperature with tetramethylsilane as an internal standard.

NMR Relaxation Study. Proton NMR measurements were carried out at 500 MHz, using a Bruker DRX499 spectrometer. The purified CYP3A4 was exchanged into deuterated 100 mM potassium phosphate at pH 7.4. The exchange buffer was previously prepared by treating a 100 mM potassium phosphate solution twice with freshly regenerated Chelex-100 to remove trace amounts of transition metals in the buffer. The treated phosphate buffer was then lyophilized and resuspended in D_2O. This was repeated 3 times to exchange the hydrogens with deuterium. The deuterated phosphate buffer was exchanged into the sample using an Amicon Ultra 10 000 MWCO spin concentrator. It was observed that, upon removing glycerol, P450 protein occasionally aggregated. DLPC or other lipids were not used because MDZ dissolved into the lipid phase, which affected T_1 values and the free substrate concentration. Similarly, NADPH−cytochrome P450 oxidoreductase was not added to samples because MDZ partitions into the lipids that aid in the reductase−CYP3A4 interaction. Samples were centrifuged to remove any aggregated protein. The sample was purged with N_2 gas to remove any dissolved oxygen in the buffer immediately before NMR spectra were taken. The sample (0.6 mL) was contained in a standard 5 mm NMR tube.

An inversion−recovery pulse sequence with 15 τ values was used to measure the observed longitudinal relaxation times ($T_{1,obs}$). The 15 τ values are as follows: 0.05, 0.1, 0.15, 0.2, 0.25, 0.3, 0.4, 0.5, 0.75, 1, 1.5, 2, 4, 6, and 8 s. The proton relaxation time measurements were carried out at a temperature of 298 K. For each τ value, 16 scans were acquired, with 4 dummy scans to reduce the proton signals from water. It was necessary to suppress the residual water proton signals via a watergate pulse sequence (*28*), which removed baseline distortions because of the water peak during the shorter time points. The signal attenuation associated with water suppression allowed us to measure the relaxation rate for only one of the C4−H protons of MDZ. A brief explanation of equations used to measure protein−heme distances is given below.

The paramagnetic contribution to the spin−lattice relaxation rate ($1/T_{1,p}$) was calculated by subtracting the relaxation rate of a diamagnetic control [$1/T_{1,obs(Fe^{2+})}$] from the relaxation rate of the paramagnetic sample [$1/T_{1,obs(Fe^{3+})}$] (*29*).

$$1/T_{1p} = 1/T_{1,obs(Fe^{3+})} - 1/T_{1,obs(Fe^{2+})} \quad (1)$$

In our experiments, the T_1 relaxation time was measured before and after conversion of the P450 to its diamagnetic sodium-dithionite-reduced carbon monoxide complex (*30*, *31*). T_{1p} may be determined in this manner because the contribution of the unbound substrate and other diamagnetic effects of substrate binding cancel out (*29*).

Demonstration of Fast Exchange. In the current study, the conditions of fast exchange were verified from the observation of chemical shifting, line broadening of the MDZ spectrum upon titration of CYP3A4, and demonstrating a positive temperature dependence on T_{1p}. T_1 measurements were performed as described above at three different temperatures (278, 288, and 298 K). Data were collected both in the absence and presence of CO/sodium dithionite. The resulting T_1 values were used to calculate T_{1p} using eq 1.

Distance Calculations. The Solomon−Bloembergen equation was used to relate paramagnetic relaxation times and distances to the paramagnetic iron (*20*, *29*, *32*).

$$\frac{1}{T_{1p}} = \left(\frac{E_0}{K_d + S_0}\right)\left(\frac{1}{T_{1m}} + \frac{1}{\tau_m}\right) \quad (2)$$

where

$$\frac{1}{T_{1m}} = \frac{2\gamma_1^2 g^2 \beta^2 S(S+1)}{15r^6}\left(\frac{3\tau_c}{1+\omega_i^2\tau_c^2} + \frac{7\tau_c}{1+\omega_s^2\tau_c^2}\right) \quad (3)$$

Here, γ_1 is the nuclear gyromagnetic ratio, g is the Landé g factor for the metal ion, β is the Bohr magneton, S is the electronic spin angular momentum quantum number of the paramagnetic center ($^5/_2$ for high- and $^1/_2$ for low-spin iron), r is the distance of the proton from the heme iron, ω_i and ω_s are the nuclear and electron Larmor frequencies, and τ_c is the correlation time of the electron and proton dipolar interaction. T_{1p} and T_{1m} are related by the percentage of substrate bound and the lifetime of the substrate−enzyme complex (*29*). Thus, the percentage of the substrate bound can be calculated from the total enzyme concentration, E_0, the dissociation constant, K_d, and the total substrate concentration, S_0. Under the conditions of fast exchange with respect to the chemical shift and nuclear relaxation, the lifetime of the substrate−enzyme complex, τ_m, is much smaller than T_{1m}, and thus, τ_m cancels in eq 2.

Equations 2 and 3 can be combined and simplified to the form presented in eq 4 if it is assumed that $\omega_i^2\tau_c^2 \ll 1$ and $\omega_s^2\tau_c^2 \gg 1$ (a reasonable approximation for hemoproteins). Here, $\gamma_1^2 g^2 \beta^2$ is equal to 2.47×10^{17} s^{-2} Å^{-6}.

$$\frac{1}{T_{1p}} = \left(\frac{E_0}{K_d + S_0}\right)\frac{9.87 \times 10^{16} S(S+1)}{r^6}(\tau_c) \qquad (4)$$

This simplified form of the Solomon−Bloemberben equation was used to calculate MDZ proton−heme iron distances. A τ_c value of 3×10^{-10} was assumed because this value corresponds to the average found for P450s in the literature and is equal to the value calculated earlier by our laboratory for CYP1A2 (*31*). Most recent τ_c values reported for P450 fall within the range from 1×10^{-10} to 6×10^{-10}. Even if the assumed τ_c values were off by a factor of 2, this error would result in a systematic 10% over- or underestimation in the calculated distance, owing to the sixth order dependence of distance on the relaxation rate.

Measurements were performed at concentrations of 0.2 μM CYP3A4 and 500 μM MDZ. MDZ concentrations were well-above the calculated K_d value of 6 μM. Optical spectroscopy indicated a mixed spin state for unbound ferric CYP3A4, with conversion to approximately 90% high spin upon the addition of 500 μM MDZ. The further addition of 50 μM testosterone or α-NF caused less than a 2% change in the spin state. Because CYP3A4 was primarily high spin for all sample conditions, a value of $S = {}^5/_2$ was used in all distance calculations. If calculations are made using 90% high spin ($S = 90\% \times {}^5/_2 + 10\% \times {}^1/_2$), reported distances decrease by 2.3%.

Modeling of MDZ with CYP3A4. The MDZ structure was drawn with ArgusLab 4.0 (Planaria Software, Seattle, WA). The geometry was optimized using the NDDO (neglect of diatomic differential overlap) semiempirical method of PM3 by steepest decent (*33*−*36*). After a reasonable geometry of MDZ was achieved, an iron atom, serving as the heme, was positioned to fit with the distances determined by NMR (Table 3). All of the distances between the iron, except for H-10, fit within 0.5 Å of the NMR measurements, giving a reasonable approximation of the orientation and distance of MDZ to the iron. MDZ and iron were then fit into the active site of the X-ray crystal structure of CYP3A4 solved by Yano et al. (*16*), using WebLab Viewer Lite 4.0 (Accelrys, formerly Molecular Simulations, Inc., San Diego, CA). MDZ was then manipulated to reduce van der Waals overlap, providing a working model of the orientation of MDZ under different conditions with the heme.

RESULTS

MDZ Kinetics. Metabolism of MDZ by CYP3A4 was found to generate two hydroxylated metabolites, 1′-hydroxy- and 4-hydroxymidazolam. The hydroxylation rates with various MDZ concentrations were used to determine K_m and V_{max} values for both reactions (Table 1). The data were fit to the Michaelis−Menten equation ($V = V_{max}[S]/(K_m + [S])$ and to an uncompetitive binding model ($V = V_{max}[S]/(K_m + [S](1 + [S]/K_i))$. The kinetics of 4-hydroxylation fit well to the Michaelis−Menten equation. The kinetics of 1′-hydroxylation were more accurately described by the uncompetitive binding equation (Figure 2). When 50 μM testosterone was present, the observed K_m for 4-hydroxylation decreased and the V_{max} slightly increased, consistent with earlier reports that testosterone favored the formation of the 4-hydroxy product (Figure 3). While the overall V_{max} and K_m are only modestly changed, the addition of testosterone led to a large increase in the formation of 4-hydroxymidazolam at lower MDZ concentrations. Addition of 50 μM α-NF resulted in a 50% increase in the V_{max} of 1′-hydroxymidazolam formation. Addition of 10 μM α-NF caused a similar stimulation in the V_{max} but caused a smaller increase in K_m.

Table 1: Kinetic Constants for MDZ Oxidation by CYP3A4

	product	K_m (μM)	V_{max}	K_i (μM)
MDZ	1′-OH[a]	11 ± 2	24 ± 2	330 ± 120
	4-OH[b]	30 ± 3	15 ± 1	n/a
MDZ +	1′-OH[a]	14 ± 1	18 ± 1	n/a
50 mM testosterone	4-OH[b]	21 ± 2	18 ± 1	n/a
MDZ +	1′-OH[a]	58 ± 5	26 ± 1	n/a
50 mM α-NF	4-OH[b]	125 ± 13	19 ± 1	n/a
MDZ +	1′-OH[a]	22 ± 2	35 ± 2	780 ± 230
10 mM α-NF	4-OH[b]	50 ± 5	17 ± 1	n/a

[a] Data fit to an uncompetitive binding model. [b] Data fit by the Michaelis−Menten equation.

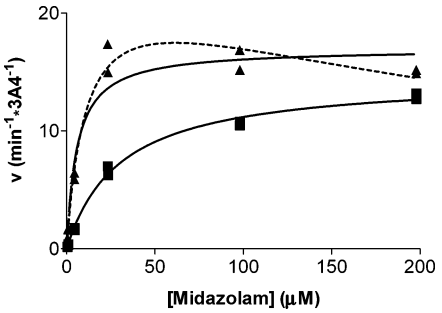

FIGURE 2: Effect of the concentration on MDZ oxidation. Incubations of reconstituted CYP3A4 with MDZ were monitored for production of both the 4-hydroxymidazolam (■) and 1′-hydroxymidazolam (▲). The data for 4-hydroxylation was curve-fit using the Michaelis−Menten equation. Data for 1′-hydroxylation was fit to both the Michaelis−Menten equation (—) and an uncompetitive binding equation (- - -).

The true kinetics of MDZ oxidation are poorly described by standard kinetic constants such as V_{max} and K_m because only 1′-hydroxylation is significantly affected by negative homotropic allosterism. Thus, at MDZ concentrations where 4-hydroxylation is nearing its V_{max}, 1′-hydroxylation is significantly inhibited. The data for the rate of 4-hydroxylation with various MDZ concentrations is shown in Figure 3A. At all MDZ concentrations examined, the rate of 4-hydroxylation was greater when 50 μM testosterone was included in the incubation. The rate of 4-hydroxylation was lower when 50 μM α-NF was included in the incubations and was minimally changed with 10 μM α-NF (although this is not reflected in the V_{max} values). The effect of α-NF on 4-hydroxylation was consistent with competitive inhibition as seen by the convergent lines on the *y* axis of the Lineweaver−Burk plot (Figure 4). The calculated K_i for α-NF on the rate of 4-hydroxylation was 72 ± 10 μM.

The kinetics of 1′-hydroxylation are dominated by the apparent negative homotropic allosterism (Figure 3B). At low MDZ concentrations (0.5, 1.0, and 5.0 μM), the rate of 1′-hydroxylation was found to be greatest when neither testosterone nor α-NF was included in the incubations. At

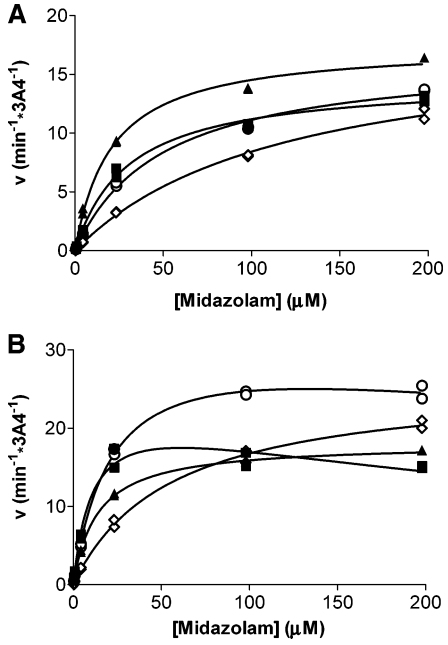

FIGURE 3: Effect of testosterone and α-NF on MDZ oxidation. Incubations of reconstituted CYP3A4 with MDZ (■) were monitored for production of both (A) 4-hydroxymidazolam and (B) 1′-hydroxymidazolam. The effect of inclusion of 50 μM testosterone (▲), 50 μM α-NF (◇), and 10 μM α-NF (○) are also depicted. The data were used to determine the kinetic constants that are given in Table 1.

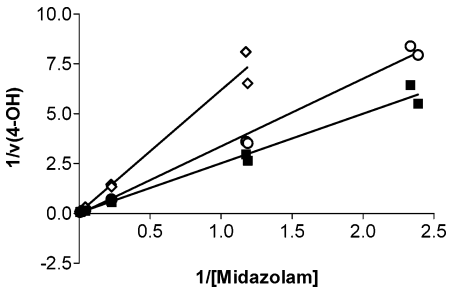

FIGURE 4: Lineweaver−Burk plot of 4-hydroxymidazolam formation in the presence of α-NF. Incubations of reconstituted CYP3A4 with MDZ (■) were monitored for production of 4-hydroxymidazolam with and without 50 μM α-NF (◇) and 10 μM α-NF (○).

MDZ concentrations above 25 μM, addition of α-NF had a positive effect on the formation rate of 1′-hydroxymidazolam. The apparent negative homotropic allosterism becomes pronounced at high MDZ concentrations. Both testosterone and α-NF appear to minimize homotropic effects at higher MDZ concentrations. Incubations that included α-NF yielded the highest rate of 1′-hydroxylation at high MDZ concentrations.

NMR Assignments. Figure 5A plots the 1D ^{1}H NMR spectra of MDZ in D_2O under acidic conditions, whereas Figure 5B plots the 1D ^{1}H NMR spectra of 500 mM MDZ with 0.2 mM CYP3A4 at pH 7.4. Assignments of MDZ proton signals were made based on the 1D spectrum presented and additional 2D ROESY, HSQC, and HMBC NMR data (not shown). MDZ has a 1′-methyl group that corresponds to a single peak at 2.49 ppm at pH 7.4 (2.74 ppm under acidic conditions). The ^{1}H signals for the doublets at 4.08 and 4.95 ppm (4.19 and 5.06 ppm under acidic conditions) were assigned to the 4-methylene group on the benzodiazepine ring based on the large geminal coupling

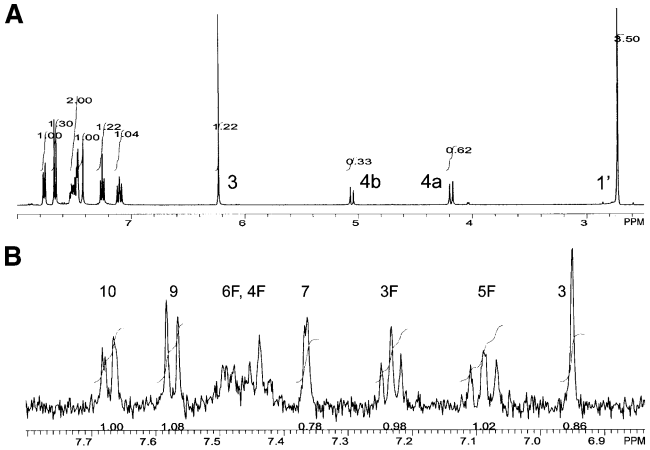

FIGURE 5: NMR spectrum of MDZ. Spectra of MDZ in D_2O under acidic conditions (A) and a blowup of the aromatic region at pH 7.4 in the presence of 0.2 μM CYP3A4 (B). Peak assignments and integration values are displayed.

(J = 14.1 Hz), a connectivity between C-4 and H-4 in the HSQC spectrum (data not shown) and a weak interaction between both 4 methylene protons and the H-3 proton in the ROESY (data not shown). Water suppression lead to bleaching around the immediate area; therefore, only one C-4 proton (4.08 ppm, furthest from the water signal) could be used for T_1 measurements. With the exception of this one resonance, all other MDZ protons could be detected and measured, and assignments for these are in Figure 5.

T_1 Experiments. To demonstrate that MDZ is in fast exchange, Figure 6A shows the ligand resonances in the aromatic region in the absence and presence of CYP3A4. Clearly, the addition of protein causes significant and varied shifts in the NMR resonances. These results are consistent with the ligand being in fast exchange with respect to the chemical shift (*37*). Further evidence of fast exchange is offered in Figure 6B, where the temperature dependence on the T_1 relaxation for the protons of the 1′-methyl group are shown. A positive slope in the double-reciprocal plot of T_{1p} versus temperature indicates that the fast exchange condition is being met. This condition also requires that double-reciprocal plots of $1/T_{1,obs(Fe^{3+})}$ versus temperature have a positive slope (*37*). The double-reciprocal plots of T_{1p} and $1/T_{1,obs(Fe^{3+})}$ versus temperature are shown in Figure 6B and support the claim that the fast-exchange requirement has been satisfied.

The observed T_1 spin-lattice relaxation times measured for the MDZ−CYP3A4 NMR sample in the presence and absence of effectors (testosterone and α-NF) are presented in Table 2, both for the paramagnetic ferric state and the diamagnetic ferrous CO-bound control state. The paramagnetic contribution to the spin-lattice relaxation rate was used to calculate MDZ proton−heme iron distances, and these distances are presented in Table 3. Weak NMR signals for testosterone and α-NF were visible when they were included. The relaxation rates of the effector molecule protons were enhanced in the presence of the paramagnetic/ferric P450. Because of low signal-to-noise ratios, T_1 values could not be calculated for individual proton peaks of either testosterone or α-NF.

Distance measurements reported in Table 3 were calculated using two MDZ dissociation constants. The distances cal-

Table 2: $T_{1,obs}$ for MDZ in the Presence of Para- and Diamagnetic CYP3A4[a]

	MDZ		MDZ + testosterone		MDZ + α-NF	
proton	$T_{1,obs(Fe^{3+})}$ (s)	$T_{1,obs(Fe^{2+}-CO)}$ (s)	$T_{1,obs(Fe^{3+})}$ (s)	$T_{1,obs(Fe^{2+}-CO)}$ (s)	$T_{1,obs(Fe^{3+})}$ (s)	$T_{1,obs(Fe^{2+}-CO)}$ (s)
H-1′	0.78	1.11	0.79	1.08	0.63	1.13
H-3	1.09	3.24	1.42	3.26	1.42	3.39
H-4(a)	0.41	0.51	0.40	0.50	0.43	0.51
H-10	1.01	1.49	1.11	1.42	1.15	1.47
H-9	1.16	2.27	1.36	2.19	1.58	2.34
H-7	1.61	4.43	1.93	4.67	2.59	4.78
H-3F	1.23	2.19	1.39	2.12	1.76	2.22
H-5F	1.12	1.96	1.31	1.84	1.60	1.92

[a] For all samples, the CYP3A4 concentration was 0.2 μM. MDZ concentrations were 500 μM, and when appropriate, 50 μM testosterone or 50 μM α-NF were added as effectors.

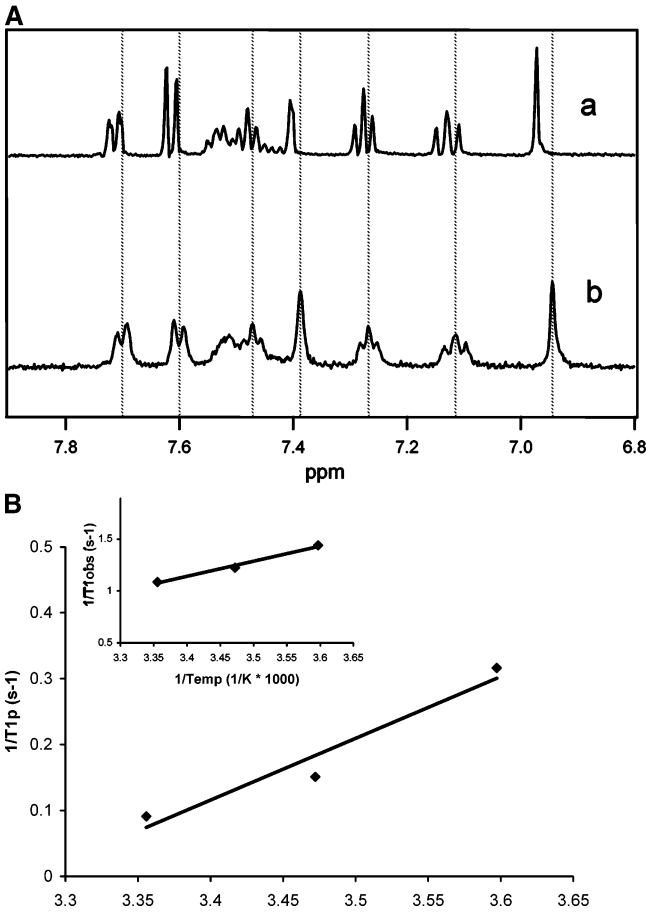

FIGURE 6: Demonstration of MDZ fast exchange with CYP3A4. (A) Observed chemical shift of the aromatic protons in the proton NMR specrum of 500 μM MDZ in phosphate buffer at pH 7.4 (a) and upon the addition of 5 μM CYP3A4 to the sample (b). (B) Temperature dependence of T_{1p} times for the 1′-methyl group of MDZ shows that a positive linear slope is indicative of fast-exchange conditions. The inset shows a plot of $T_{1,obs}$ versus 1/temp.

culated for K_d = 6 μM are based on the experimentally determined K_d from spin-state changes when CYP3A4 was titrated with MDZ. Both 50 μM α-NF and 50 μM testosterone induced high-spin transitions in CYP3A4, and dissociation constants could not be calculated for MDZ by the spin-state change when α-NF and testosterone were present. Because binding is likely to be affected by the presence of effector molecules, distances were also calculated using the K_m values determined by kinetic analysis. As can be seen in Table 3, calculated distances were minimally affected.

In the absence of the effector molecule, NMR T_1 paramagnetic relaxation experiments generated a uniform set of MDZ proton−heme iron distances, suggesting significant MDZ movement within the active site and no favored binding orientation. In the presence of α-NF, NMR T_1 paramagnetic relaxation experiments generated a skewed distribution of MDZ proton−heme iron distances, with the C1′−H MDZ proton significantly decreased in distance from 8.0 ± 0.2 to 7.3 ± 0.1 Å. In addition, the distances to the protons on the flourophenyl ring of MDZ increased significantly from 8.0 ± 0.4 to 10.0 ± 0.6 Å for C5-H, suggesting that the fluorophenyl ring is orientated away from the heme iron. A closest approach of the C1′-H MDZ proton to the heme is consistent with experimentally determined kinetics, showing C1′ to be the favored site of oxidation in the presence of α-NF. In the presence of testosterone, a less striking change in distances was observed, although C4-H was closest to the heme iron (7.7 ± 0.3 Å, Table 3), consistent with C4 as the favored site of oxidation.

Table 3: Calculated Distances between MDZ Protons and Heme Iron[a]

	MDZ	MDZ + testosterone		MDZ + α-NF	
proton	Å	Å, if K_d = 6 μM	Å, if K_d = 14 μM	Å, if K_d = 6 μM	Å, if K_d = 58 μM
H-1′	8.0 ± 0.2	8.2 ± 0.2	8.2 ± 0.2	7.3 ± 0.1	7.1 ± 0.1
H-3	7.4 ± 0.2	8.0 ± 0.2	8.0 ± 0.2	7.9 ± 0.3	7.8 ± 0.3
H-4(a)	7.8 ± 0.4	7.7 ± 0.3	7.7 ± 0.3	8.1 ± 0.4	8.0 ± 0.4
H-10	8.3 ± 0.4	8.5 ± 0.3	8.4 ± 0.3	9.0 ± 0.6	8.9 ± 0.6
H-9	7.9 ± 0.4	9.0 ± 0.4	8.9 ± 0.4	8.9 ± 0.4	8.8 ± 0.4
H-7	8.0 ± 0.2	8.3 ± 0.2	8.3 ± 0.2	9.1 ± 0.2	9.0 ± 0.2
H-3F	8.1 ± 0.5	8.6 ± 0.4	8.6 ± 0.4	9.8 ± 0.4	9.6 ± 0.4
H-5F	8.0 ± 0.4	8.8 ± 0.5	8.8 ± 0.5	10.0 ± 0.6	9.8 ± 0.5

[a] Distances were calculated using a K_d value of 6 μM. Distances were also calculated in the + testosterone and + α-NF columns using K_d values of 14 and 58 μM, respectively (the calculated K_m values for MDZ oxidation in the presence of testosterone or α-NF).

On the basis of the calculated distances, a theoretical geometry is suggested in Figure 7. The structural model is presented to aid in visualizing possible changes in MDZ active-site orientation. All geometries presented in Figure 7 were fit to the active site of CYP3A4 based on the X-ray crystal structure (*16*) and minimized for van der Waals overlap. The structure assumes that the heme iron can be treated as a point source, which is not strictly true, but we believe discrepancies will be small. Even if delocalization of the paramagnetic heme electrons are more prominent than anticipated, this will not alter the main conclusion: that MDZ orientation is altered by the presence of the effector molecules.

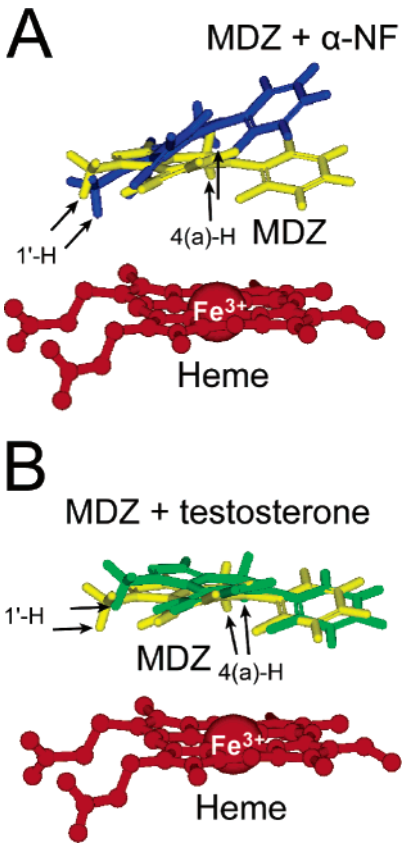

FIGURE 7: Hypothetical models of MDZ orientations above heme in the CYP3A4 active site in the absence and presence of effectors. (A) MDZ bound to CYP3A4 alone (yellow) and in the presence of α-NF (blue). (B) MDZ bound to CYP3A4 alone (yellow) and in the presence of testosterone (green).

DISCUSSION

The kinetics of MDZ oxidation are complicated by several factors. First, CYP3A4 is inactivated during the course of the incubation (*12*). A reactive intermediate in the formation of the 1′-hydroxy metabolite has been proposed to be responsible. Few studies, including this one, have accounted for this reactive intermediate in their kinetic analysis but have instead looked at the total metabolites formed and divided by the total incubation time to derive rates. To decrease the effect of inactivation, we have shortened our incubation times to 3 min. However, because of inactivation, V_{max} values reported herein are probably lower than the true initial velocities of MDZ oxidation. Also affecting the kinetics is the low K_m and high turnover of MDZ. Because of this, the concentration of substrate changes over the course of the incubation. Fitting this second-order reaction to first-order kinetic equations causes an inherent error in analysis. We have used the average MDZ concentration over the course of the reaction to decrease this error. Finally, fitting the 1′-hydroxylation data to the standard Michaelis−Menten equation causes a large error in both V_{max} and K_m. Curve fitting that accounts for uncompetitive binding gives rates much more representative of the observed data.

Our kinetic data for MDZ oxidation are consistent with reports in the literature. Using reconstituted recombinant protein, Khan et al. reported a 3:1 ratio of 1′-hydroxymidazolam/4-hydroxymidazolam at 25 μM MDZ and a 1:1 ratio at 250 μM MDZ (*12*). We found ratios of 2.5:1 and 1:1 at similar concentrations. Wang et al. reported that incubation of 25 μM MDZ and 50 μM testosterone with human liver microsomes yielded an 80% increase in the velocity of 4-OH formation over the control without testosterone (*37*). We found a 40% increase under similar conditions. Wang et al. also reported a 15% decrease in the rate of 4-hydroxymidazolam in the presence of 10 μM α-NF and a 40% decrease with 50 μM α-NF (*38*). We found decreases of 15 and 50% under similar conditions.

Literature reports with respect to 1′-hydroxylation are contradictory. The majority of researchers have seen a decrease in the rate of 1′-hydroxylation at higher MDZ concentrations, similar to our observations. Wang et al. reported a 25% decrease in the rate of 1′-hydroxylation with 25 μM MDZ and 50 μM testosterone, which agrees well with our observed 30% decrease in the rate. However, our results with α-NF contrast with the results of both Wang et al. (*38*) and Maenpaa et al. (*39*), who both report stimulation of 1′-hydroxylation with 25 μM MDZ and α-NF. We found that α-NF decreased or eliminated the negative homotropic allosterism, accounting for the drop in velocity at high MDZ concentrations. Because of this, the rate of 1′-hydroxylation in the presence of α-NF was increased at high MDZ concentrations but not at concentrations of 25 μM or below. The results of Ghosal et al. (*40*) more closely matched our findings. They found that α-NF stimulated the rate of 1′-hydroxymidazolam formation only at low α-NF concentrations when 64 μM MDZ was incubated with human liver microsomes.

Our kinetic results are consistent with at least two MDZ-binding orientations, one that favors oxidation at the C1′ position and one that favors oxidation at the C4 position. Oxidation at the C1′ position was inhibited by high MDZ concentrations, consistent with a negative allosteric effect. The addition of α-NF decreased the negative allosteric effect on the rate of 1′-hydroxylation by the proposed second molecule of MDZ. α-NF competitively inhibited formation of the 4-hydroxy metabolite, implying that α-NF occupies the preferred site for 4-hydroxymidazolam formation. The interaction or overlap of two MDZ-binding sites may be responsible for the negative homotropic kinetics of 1′-hydroxymidazolam formation, but this interaction is not straightforward because the K_i for noncompetitive binding is much greater than the K_m for 4-hydroxylation.

While information about binding and substrate orientation within the CYP3A4 active site is discernible from kinetics, the possibility of stabilization of intermediates and regional structural changes upon binding of the effector to a distal site outside of the binding pocket are not easily discernible from the substrate and effector bound within the active site. NMR T_1 paramagnetic relaxation experiments offer an alternative nonkinetic approach to the study of heterotropic allosteric interactions. Both sites of MDZ hydroxylation were followed, and changes in the MDZ orientation were determined upon addition of testosterone and α-NF that agreed with kinetic results for the favored site of oxidation.

The optimal proton−heme iron distance for hydrogen extraction would be approximately 5 Å. This is based on an assumption of an iron−oxygen bond distance of 1.8 Å and sufficient molecular orbital overlap for hydrogen atom extraction from the substrate by the perferryl oxygen. Distances calculated in this study were 2−3 Å longer. The reason for this is not obvious, and we propose two possibili-

ties. First, there is precedence with P450 μ_B3 for substrate movement of up to 6 Å after reduction of the heme iron (*41*). A second explanation is related to protein aggregation. Because MDZ partitions into the lipid phase, exogenous lipids could not be added to prevent aggregation. To control protein aggregation, we kept protein levels low and centrifuged the samples prior to the experiments to remove the small amount of aggregate. We then quantitated the P450 by spectroscopy and adjusted the volume to achieve the desired concentration. If there were microaggregates that could not be removed by centrifugation, the effective concentration of CYP3A4 could have been reduced, resulting in longer calculated distances to all MDZ protons. All distance calculations would scale by a consistent percentage without changing the relative positioning of the MDZ molecule.

Similar although opposite effects were recently shown for the interaction of flurbiprofen and dapsone within the CYP2C9 active site. The authors show quite convincingly that the addition of dapsone caused the reorientation of flurbiprofen within the CYP2C9 active site (*23*). However, the calculated proton−heme iron distances were between 3.16 and 3.79 Å. Given the 1.8 Å iron−oxo bond, most of the flurbiprofen protons would be too close for even covalent binding let alone hydrogen extraction. The data from the flurbiprofen study along with the data presented here illustrates that paramagnetic relaxation studies are best at illustrating global changes and not for discrete distance calculations.

In the absence of either effector molecule, NMR T_1 paramagnetic relaxation experiments generated a uniform set of MDZ proton−heme iron distances. The uniformity of the distances in the absence of the effector indicates a nonfavored orientation for binding. Several models can be invoked to account for this, including unhindered rotation of the MDZ molecule within the active site, exchange between multiple but discrete MDZ-binding sites, or sliding of the MDZ molecule along the heme plane.

In the presence of testosterone, longer distances from the heme iron to the chloro- and flouro-ring protons were determined. It is possible that the MDZ is forced to bind to a different region within the CYP3A4 active site or that the ability of MDZ to slide along the heme plane is restricted when testosterone is present. The $T_{1,obs}$ for testosterone was found to be affected by the paramagnetic heme iron, indicating that both testosterone and MDZ bound in proximity to the heme iron. Testosterone and MDZ were not found to be competing for a single binding site. If there was competition for one site, the calculated proton−heme iron distances should have uniformly increased as more MDZ was displaced from the pocket, leading to a lower percentage of MDZ bound near the paramagnetic heme iron. Kinetic measurements also argue against single-site competition because at high MDZ concentrations testosterone increased the rate of 4-OH formation without negatively affecting 1′-OH metabolite formation. Induced orientation changes by testosterone are relatively small and only slightly favor 4-OH formation. However, only the C4 proton−heme iron distance of the nonoxygenated P450−substrate complex can be measured in these NMR studies, which may not accurately reflect substrate proton distances to the reactive oxygen species.

In the presence of α-NF, the distance of the heme iron to the C1′-H MDZ proton was significantly decreased from 8.0 ± 0.2 to 7.3 ± 0.1 Å and the C5-H of the fluorophenyl ring significantly increased from 8.0 ± 0.4 to 10.0 ± 0.6 Å. This new set of distances suggests a favored orientation of the MDZ molecule, with the fluorophenyl ring situated further away from the heme iron than the benzodiazepine ring (Figure 7). This orientation is consistent with experimentally determined kinetics, showing the C1′-H to be the favored site of oxidation in the presence of α-NF. It is easy to envision that this preferred orientation to the heme is the reason for the observed kinetic changes in the presence of α-NF.

The adoption of what appears to be a favored orientation for bound MDZ in the presence of the effector could be explained if the cobinding of effector were to lead to steric crowding and restriction of either the rotational or translational components of motion for MDZ within the CYP3A4 active site. Such a model is suggested by the crystallographic work of Cupp-Vickery et al. (*42*), who have shown co-occupancy of two substrate molecules within the active site of cytochrome P450eryF. Binding of the effector to distal sites on the surface of the enzyme might also account for the existence of a favored binding orientation for MDZ, provided that effector binding was accompanied by a significant conformational change in CYP3A4 active-site architecture. However, our T_1 paramagnetic relaxation measurements of α-NF and testosterone resonances in the MDZ/CYP3A4 NMR sample clearly show enhanced relaxation rates for these resonances. Detailed measurements were not possible for the individual protons of α-NF and testosterone because of limited signal-to-noise ratios, but the signals were clearly relaxing faster as seen by more rapid inversion of the signals through the zero point (data not shown), indicating that both α-NF and testosterone bind in the vicinity of the heme iron in the presence of MDZ.

In summary, while work remains to explain allosterism in CYP3A4, our results demonstrate for the first time, using an NMR method, that the presence of an effector can induce changes in the geometry of substrate binding in CYP3A4.

ACKNOWLEDGMENT

The authors thank Dr. Dolores Diaz for her help with and discussions about methods of water suppression.

REFERENCES

1. Lasker, J. M., Huang, M. T., and Conney, A. H. (1982) *In vivo* activation of zoxazolamine metabolism by flavone, *Science 216*, 1419−1421.
2. Schwab, G. E., Raucy, J. L., and Johnson, E. F. (1988) Modulation of rabbit and human hepatic cytochrome P-450-catalyzed steroid hydroxylations by α-naphthoflavone, *Mol. Pharmacol. 33*, 493−499.
3. Shou, M., Grogan, J., Mancewicz, J. A., Krausz, K. W., Gonzalez, F. J., Gelboin, H. V., and Korzekwa, K. R. (1994) Activation of CYP3A4: Evidence for the simultaneous binding of two substrates in a cytochrome P450 active site, *Biochemistry 33*, 6450−6455.
4. Harlow, G. R., and Halpert, J. R. (1998) Analysis of human cytochrome P450 3A4 cooperativity: Construction and characterization of a site-directed mutant that displays hyperbolic steroid hydroxylation kinetics, *Proc. Natl. Acad. Sci. U.S.A. 95*, 6636−6641.
5. Shou, M., Mei, Q., Ettore, M. W., Jr., Dai, R., Baillie, T. A., and Rushmore, T. H. (1999) Sigmoidal kinetic model for two co-operative substrate-binding sites in a cytochrome P450 3A4

active site: An example of the metabolism of diazepam and its derivatives, *Biochem. J. 340*, 845−853.
6. Hosea, N. A., Miller, G. P., and Guengerich, F. P. (2000) Elucidation of distinct ligand binding sites for cytochrome P450 3A4, *Biochemistry 39*, 5929−5939.
7. Emoto, C., Yamazaki, H., Iketaki, H., Yamasaki, S., Satoh, T., Shimizu, R., Suzuki, S., Shimada, N., Nakajima, M., and Yokoi, T. (2001) Cooperativity of α-naphthoflavone in cytochrome P450 3A-dependent drug oxidation activities in hepatic and intestinal microsomes from mouse and human, *Xenobiotica 31*, 265−275.
8. Kenworthy, K. E., Clarke, S. E., Andrews, J., and Houston, J. B. (2001) Multisite kinetic models for CYP3A4: Simultaneous activation and inhibition of diazepam and testosterone metabolism, *Drug Metab. Dispos. 29*, 1644−1651.
9. Lu, P., Lin, Y., Rodrigues, A. D., Rushmore, T. H., Baillie, T. A., and Shou, M. (2001) Testosterone, 7-benzyloxyquinoline, and 7-benzyloxy-4-trifluoromethyl-coumarin bind to different domains within the active site of cytochrome P450 3A4, *Drug Metab. Dispos. 29*, 1473−1479.
10. Shou, M., Dai, R., Cui, D., Korzekwa, K. R., Baillie, T. A., and Rushmore, T. H. (2001) A kinetic model for the metabolic interaction of two substrates at the active site of cytochrome P450 3A4, *J. Biol. Chem. 276*, 2256−2262.
11. Galetin, A., Clarke, S. E., and Houston, J. B. (2002) Quinidine and haloperidol as modifiers of CYP3A4 activity: Multisite kinetic model approach, *Drug Metab. Dispos. 30*, 1512−1522.
12. Khan, K. K., He, Y. Q., Domanski, T. L., and Halpert, J. R. (2002) Midazolam oxidation by cytochrome P450 3A4 and active-site mutants: An evaluation of multiple binding sites and of the metabolic pathway that leads to enzyme inactivation, *Mol. Pharmacol. 61*, 495−506.
13. Torimoto, N., Ishii, I., Hata, M., Nakamura, H., Imada, H., Ariyoshi, N., Ohmori, S., Igarashi, T., and Kitada, M. (2003) Direct interaction between substrates and endogenous steroids in the active site may change the activity of cytochrome P450 3A4, *Biochemistry 42*, 15068−15077.
14. Guengerich, F. P. (1995) Cytochrome P450 enzymes, *Cytochrome P450: Structure, Mechanism, and Biochemistry* (Ortiz de Montellano, P. R., Ed.) pp 473−536, Plenum Press, New York.
15. Williams, P. A., Cosme, J., Vinkovic, D. M., Ward, A., Angove, H. C., Day, P. J., Vonrhein, C., Tickle, I. J., and Jhoti, H. (2004) Crystal structures of human cytochrome P450 3A4 bound to metyrapone and progesterone, *Science 305*, 683−686.
16. Yano, J. K., Wester, M. R., Schoch, G. A., Griffin, K. J., Stout, C. D., and Johnson, E. F. (2004) The structure of human microsomal cytochrome P450 3A4 determined by X-ray crystallography to 2.05 Å resolution, *J. Biol. Chem. 279*, 38091−38094.
17. Dabrowski, M. J., Schrag, M. L., Wienkers, L. C., and Atkins, W. M. (2002) Pyrene−pyrene complexes at the active site of cytochrome P450 3A4: Evidence for a multiple substrate binding site, *J. Am. Chem. Soc. 124*, 11866−11867.
18. Korzekwa, K. R., Krishnamachary, N., Shou, M., Ogai, A., Parise, R. A., Rettie, A. E., Gonzalez, F. J., and Tracy, T. S. (1998) Evaluation of atypical cytochrome P450 kinetics with two-substrate models: Evidence that multiple substrates can simultaneously bind to cytochrome P450 active sites, *Biochemistry 37*, 4137−4147.
19. Miller, J. C., Lohr, L. L., and Sharp, R. R. (2001) NMR paramagnetic relaxation enhancement: Test of the controlling influence of zfs rhombicity for $S = 1$, *J. Magn. Reson. 148*, 267−276.
20. Strandberg, E., and Westlund, P. (1999) Paramagnetic proton nuclear spin relaxation theory of low-symmetry complexes for electron spin quantum number $S = {}^5/_2$, *J. Magn. Reson. 137*, 333−344.
21. Modi, S., Primrose, W. U., Boyle, J. M., Gibson, C. F., Lian, L. Y., and Roberts, G. C. (1995) NMR studies of substrate binding to cytochrome P450 μ_B3: Comparisons to cytochrome P450 cam, *Biochemistry 34*, 8982−8988.
22. Koerts, J., Rietjens, I. M., Boersma, M. G., and Vervoort, J. (1995) ^{1}H NMR T_1 relaxation rate study on substrate orientation of fluoromethylanilines in the active sites of microsomal and purified cytochromes P450 1A1 and 2B1, *FEBS Lett. 368*, 279−284.
23. Hummel M. A., Gannett P. M., Aguilar J. S., and Tracy T. S. (2004) Effector-mediated alteration of substrate orientation in cytochrome P450 2C9, *Biochemistry 43*, 7207−7214.
24. Gillam, E. M., Baba, T., Kim, B. R., Ohmori, S., and Guengerich, F. P. (1993) Expression of modified human cytochrome P450 3A4 in *Escherichia coli* and purification and reconstitution of the enzyme, *Arch. Biochem. Biophys. 305*, 123−131.
25. Holmans, P. L., Shet, M. S., Martin-Wixtrom, C. A., Fisher, C. W., and Estabrook, R. W. (1994) The high-level expression in *Escherichia coli* of the membrane-bound form of human and rat cytochrome *b*5 and studies on their mechanism of function, *Arch. Biochem. Biophys. 312*, 554−565.
26. Chen, W., Koenigs, L. L., Thompson, S. J., Peter, R. M., Rettie, A. E., Trager, W. F., and Nelson, S. D. (1998) Oxidation of acetaminophen to its toxic quinone imine and nontoxic catechol metabolites by baculovirus-expressed and purified human cytochromes P450 2E1 and 2A6, *Chem. Res. Toxicol. 11*, 295−301.
27. Shaw, P. M., Hosea, N. A., Thompson, D. V., Lenius, J. M., and Guengerich, F. P. (1997) Reconstitution premixes for assays using purified recombinant human cytochrome P450, NADPH−cytochrome P450 reductase, and cytochrome *b*5, *Arch. Biochem. Biophys. 348*, 107−115.
28. Piotto, M., Saudek, V., and Sklenar, V. (1992) Gradient-tailored excitation for single-quantum NMR spectroscopy of aqueous solutions, *J. Biomol. NMR 2*, 661−665.
29. Villafranca, J. J. (1989) Paramagnetic probes of macromolecules, *Methods Enzymol. 177*, 403−413.
30. Myers, T. G., Thummel, K. E., Kalhorn, T. F., and Nelson, S. D. (1994) Preferred orientations in the binding of 4′-hydroxyacetanilide (acetaminophen) to cytochrome P450 1A1 and 2B1 isoforms as determined by ^{13}C and ^{15}N NMR relaxation studies, *J. Med. Chem. 37*, 860−867.
31. Regal, K. A., and Nelson, S. D. (2000) Orientation of caffeine within the active site of human cytochrome P450 1A2 based on NMR longitudinal (T_1) relaxation measurements, *Arch. Biochem. Biophys. 384*, 47−58.
32. Solomon, I. (1955) Relaxation processes in a system of two spins, *Phys. Rev. 99*, 559−565.
33. Dewar, M. J. S., and Thiel, W. (1977) Ground states of molecules. The MNDO method. Approximations and parameters, *J. Am. Chem. Soc. 99*, 4899−4907.
34. Stewart, J. J. P. (1989) Optimization of parameters for semiempirical methods. I. Method, *J. Comput. Chem. 10*, 209−220.
35. Pople, J. A., and Segal, G. A. (1965) Approximate self-consistent molecular orbital theory. II. Calculations with complete neglect of differential overlap, *J. Chem. Phys. 43*, S136−S149.
36. Pople, J. A., and Segal, G. A. (1965) Approximate self-consistent molecular orbital theory. I. Invariant procedures, *J. Chem. Phys. 43*, S129−S135.
37. Levitt, M. H. (2001) *Spin Dynamics: Basics of Nuclear Magnetic Resonance*, John Wiley and Sons, Ltd., New York.
38. Wang, R. W., Newton, D. J., Liu, N., Atkins, W. M., and Lu, A. Y. (2000) Human cytochrome P-450 3A4: *In vitro* drug−drug interaction patterns are substrate-dependent, *Drug Metab. Dispos. 28*, 360−366.
39. Maenpaa, J., Hall, S. D., Ring, B. J., Strom, S. C., and Wrighton, S. A. (1998) Human cytochrome P450 3A (CYP3A) mediated midazolam metabolism: The effect of assay conditions and regioselective stimulation by α-naphthoflavone, terfenadine, and testosterone, *Pharmacogenetics 8*, 137−155.
40. Ghosal, A., Satoh, H., Thomas, P. E., Bush, E., and Moore, D. (1996) Inhibition and kinetics of cytochrome P4503A activity in microsomes from rat, human, and cDNA-expressed human cytochrome P450, *Drug Metab. Dispos. 24*, 940−947.
41. Modi, S., Sutcliffe, M. J., Primrose, W. U., Lian L. Y., and Roberts, G. C. (1996) The catalytic mechanism of cytochrome P450 μ_B3 involves a 6 Å movement of the bound substrate on reduction, *Nat. Struct. Biol. 3*, 414−417.
42. Cupp-Vickery, J., Anderson, R., and Hatziris, Z. (2000) Crystal structures of ligand complexes of P450eryF exhibiting homotropic cooperativity, *Proc. Natl. Acad. Sci. U.S.A. 97*, 3050−3055.

BI051689T